Full-Wave Analysis of Three-Dimensional Planar Structures

Alexander M. Lerer and Alexander G. Schuchinsky

I. Introduction

THE development of microwave and millimeter-wave integrated circuits (MIC) is difficult to imagine now beyond reliable and efficient numerical simulation of wave interactions in real structures. To meet the challenge, sophisticated CAD tools based on the methods of field theory acquire a particular significance [1]–[5].

Many empirical and rigorous models of the discontinuities in planar microwave circuits have been elaborated during the past decade. The merits of the available approaches have been discussed in [2]. The finite-difference time domain method and a spectral domain analysis were only found to be appropriate to fulfill the tough requirements of accuracy and flexibility of numerical simulation. The former technique has the advantage in versatility but its implementation needs the most powerful modern computers with huge resources [1], [2]. Conversely, the spectral domain analysis [3]–[5] substantially reduces a numerical effort by virtue of analytically handling the problem as far as possible. Although the latter technique constrains the flexibility of simulation, most of the problems associated with planar discontinuities are proved to be amenable to rigorous numerical-analytical analysis.

The Galerkin method in spectral domain is currently the very basic approach to the problem of irregular planar structures. The expansion basis used is known (e.g. [2]–[7]) to be a crucial factor in its accuracy and convergence. A proper choice of basis functions is based on the physical reasons that impose the certain edge conditions on the field behavior near the verges of discontinuity. To the authors' knowledge the complete orthonormalized sets of the pertinent basis functions are available only for the configurations containing infinitesimally thin perfect conductors of such simple shapes as rectangle [8], circle [9], and ring [10]. For discontinuities of other specific or arbitrary shape, the expansion bases—such as finite-element polynomials and the piece-wise sinusoidal or roof-top functions—are usually used [2], [6], [11], [12]. Even though the latter bases have extended the flexibility of the technique, they dramatically degrade its computational efficiency.

The most time-consuming step of the numerical procedure based on Galerkin's method in spectral domain is evaluation of the matrix elements of the algebraic system. They used to be expressed by slowly convergent double infinite integrals or sums, and the accuracy of their computation affects substantially the precision of final solutions. This important aspect of the technique has been largely neglected in the available publications. It was only mentioned in [13] and [2], [12] with respect to the use of roof-top basis functions.

To address the above inadequacies, this paper presents an efficient numerical-analytical approach to analysis of planar and waveguide three-dimensional structures. In order to maintain high accuracy and fast convergence of solutions, the technique based on Galerkin's method in spectral domain have been developed. The advance has been achieved in the following basic points:

i) formulation of diagonalized set of integral equations for the problems associated with planar structures on multilayered uniaxial dielectric substrates;

ii) development and application of complete orthonormalized sets of basis functions accounting the edge conditions in explicit form; and

iii) devising the efficient numerical quadratures for evaluating infinite singular integrals and improvement of convergency of the integrals and series in the matrix elements of the algebraic system.

Applications of the developed approach are exemplified by numerical results for several resonant and discontinuous planar structures and rectangular waveguides coupled via a hole.

The new potentiality of the technique is demonstrated with respect to analysis of volume dielectric resonators and discontinuous structures. The advantages of the approximate quasi-planar (QP) model proposed herein are extensively discussed.

II. Formulation of Boundary Value Problem

Let us consider a flat discontinuity S placed upon a multilayered ferrite-dielectric substrate (Fig. 1). S is formed by an impedance patch or aperture in the impedance coating. The ferrite layer can be magnetized along any coordinate axis (x, y or z) and characterized by the Polder tensor $\hat{\mu}$. The substrate may be of either infinite lateral extent or confined by a shielding box. In addition, conductive planes are assumed to be above and below the substrate.

The advantages of the spectral domain approach have been taken to tackle the boundary value problem associated with the structure in Fig. 1. The technique is equally applicable to both opened and shielded configurations. Their treatment differs only in implicating the integral or discrete form of Fourier transformation, respectively. An integral formulation related to laterally unbounded structure is derived herein. However,

Manuscript received August 20, 1991; revised February 11, 1993.

The authors are with the Microwave Electrodynamics Laboratory at Rostov State University.

IEEE Log Number 9212734.

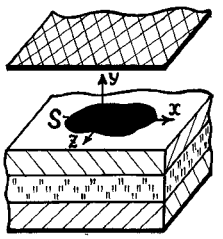

Fig. 1.

the set of dual integral equations (2) or (19), (20) for a shielded configuration can be readily rearranged to summator equations by formal merging the integration into a summation

$$\frac{1}{2\pi}\int_{-\infty}^{+\infty}\exp\{i\alpha x\}\,d\alpha \to \frac{1}{L}\sum_{n=-\infty}^{\infty}\exp\{i\alpha_n x\} \qquad (1)$$

where $\alpha_n = 2\pi n/L$ and L is the size of a shielding box with respect to the x-direction.

The boundary value problem above handled in the framework of a standard spectral domain approach [3]–[5] give rise to the matrix set of dual integral equations

$$\begin{aligned}&\iint_{-\infty}^{+\infty}\hat{G}(\alpha,\beta)\eta(\alpha,\beta)\exp\{i(\alpha x+\beta z)\}/\rho^2\,d\alpha\,d\beta - \\ &\qquad\qquad \tilde{\eta}(x,z)/Y = \xi^s(x,z), \qquad \{x,z\}\in S \\ &\iint_{-\infty}^{+\infty}\eta(\alpha,\beta)\exp\{i(\alpha x+\beta z)\}\,d\alpha\,d\beta = 0, \qquad \{x,z\}\notin S\end{aligned} \qquad (2)$$

where $\rho^2 = \alpha^2+\beta^2$; $\eta(\alpha,\beta) = \{\eta_z(\alpha,\beta),\eta_x(\alpha,\beta)\}$ is a vector of Fourier transforms of unknown surface electric/magnetic current $\tilde{\eta}(x,z)$ on S; Y is a surface admittance/impedance (for perfect conductor $Y=\infty$); vector $\xi^s(x,z)$ corresponds to the tangential field of incident wave. The kernel $\hat{G}(\alpha,\beta)$ is the Fourier transform of dyadic Green's function that relates surface electric/magnetic current to the tangential components of an electric/magnetic field at the plane $y=0$. The expression of $\hat{G}(\alpha,\beta)$ for magnetized ferrite substrate is a bit too cumbersome and omitted here. The reader is referred to [14] where the formulas have been obtained and discussed in detail. In the case of the substrate comprising a few uniaxial anisotropic dielectric layers[1] $\hat{G}(\alpha,\beta)$ can be put in more compact form (compare with [4])

$$\begin{aligned}G_{zz}(\alpha,\beta) &= \beta^2/\varphi_m(\rho) - k_0^2\alpha^2/\varphi_e(\rho),\\ G_{zx}(\alpha,\beta) &= G_{xz}(\alpha,\beta) = -\alpha\beta\{1/\varphi_m(\rho)+k_0^2/\varphi_e(\rho)\},\\ G_{xx}(\alpha,\beta) &= \alpha^2/\varphi_m(\rho) - k_0^2\beta^2/\varphi_e(\rho),\end{aligned} \qquad (3)$$

where $k_0 = \omega\sqrt{\varepsilon_0\mu_0}$ is a wavenumber of free space and $\omega = 2\pi f$, f is frequency; the functions $\varphi_{e,m}(\rho)$ defined in (15) are related to the LSE and LSM modes in the multilayered substrate, respectively.

The kernel (3) is quite remarkable in that it admits rearrangement (2) to a diagonalized set of integral equations. Such a formulation can be obtained by a direct handling (2). However, an alternative derivation proceeding immediately from the original boundary value problem (see [15]) seems to be more convenient.

Let an impedance patch S be supported by multilayered dielectric substrate (Fig. 1). Then the tangential components of magnetic $\boldsymbol{H}_{z,x}$ and electric $\boldsymbol{E}_{z,x}$ fields meet the following boundary conditions at the plane $y=0$:

$$\boldsymbol{E}_{x,z}(x,z) = \tilde{\eta}_{x,z}(x,z)/Y, \qquad \{x,z\}\in S \qquad (4)$$

$$\tilde{\eta}_{x,z}(x,z) = 0, \qquad \{x,z\}\notin S \qquad (5)$$

where

$$\tilde{\eta}_{x,z}(x,z) = \pm[\boldsymbol{H}_{z,x}(x,+0,z) - \boldsymbol{H}_{z,x}(x,+0,z)]\,. \qquad (6)$$

Referring to the arrangement of the structure in question we observe that the fields are expressible in the terms of LSE and LSM modes, which can be described by y-directed Hertzian's potentials $\Pi^{e,m}(x,y,z)$, respectively. Each of these modes satisfies the boundary conditions at the homogeneous interfaces of slabs but their superposition must be used to meet the piecewise boundary conditions (4), (5) at the plane $y=0$. The functions $\Pi^{e,m}(x,y,z)$ fulfilling the above stipulations can be put in the form

$$\begin{aligned}&\Pi^{e,m}(x,y,z) = \frac{1}{4\pi^2}\\ &\iint_{-\infty}^{+\infty}a^{e,m}(\alpha,\beta)\frac{\boldsymbol{P}^{e,m}(\rho,y)}{\boldsymbol{P}_1^{e,m}(\rho)}\exp\{i(\alpha x+\beta z)\}\,d\alpha\,d\beta\,,\end{aligned} \qquad (7)$$

where

$$\begin{aligned}&\rho^2 = \alpha^2+\beta^2;\\ &\boldsymbol{P}_1^e(\rho) = \boldsymbol{P}^e(\rho,y=0), \qquad \boldsymbol{P}_1^m(\rho) = \frac{\partial\boldsymbol{P}^m(\rho,y=0)}{\partial y}\end{aligned} \qquad (8)$$

$\boldsymbol{P}^{e,m}(\rho,y)$ are the eigenfunctions of multilayered plane waveguide of Fig. 1 outside the patch S (the functions $\boldsymbol{P}^{e,m}(\rho,y)$ satisfy the same homogeneous boundary conditions on the tangential field continuity at the plane $y=0$ as they are at the other layer interfaces). To recover functions $a^{e,m}(\alpha,\beta)$ being as yet unknown and fulfill the boundary conditions (4), (5), we express $\tilde{\eta}_{x,z}(x,z)$ and $\boldsymbol{E}_{x,z}(x,z)$ at the plane $y=0$ in the terms of $\Pi^{e,m}(x,y,z)$

$$\begin{aligned}\boldsymbol{E}_x(x,z) &= \frac{\partial\boldsymbol{F}^e(x,z)}{\partial z} - \frac{\partial\boldsymbol{F}^m(x,z)}{\partial x}\\ \boldsymbol{E}_z(x,z) &= -\frac{\partial\boldsymbol{F}^e(x,z)}{\partial x} - \frac{\partial\boldsymbol{F}^m(x,z)}{\partial z}\end{aligned} \qquad (9)$$

$$\begin{aligned}\tilde{\eta}_x(x,z) &= \frac{\partial\boldsymbol{V}^m(x,z)}{\partial x} - \frac{\partial\boldsymbol{V}^e(x,z)}{\partial z}\\ \tilde{\eta}_z(x,z) &= \frac{\partial\boldsymbol{V}^m(x,z)}{\partial z} + \frac{\partial\boldsymbol{V}^e(x,z)}{\partial x}\end{aligned} \qquad (10)$$

[1]The dielectric slabs are characterized by the diagonal tensor permittivity $\hat{\varepsilon}$ with nonzero components ε_{yy} and $\varepsilon_{xx} = \varepsilon_{zz}$.

where

$$\begin{aligned}
\boldsymbol{F}^e(x,z) &= \Pi^e(x,0,z);\\
\boldsymbol{F}^m(x,z) &= \frac{i}{\omega\varepsilon}\frac{\partial\Pi^m(x,y=0,z)}{\partial y};\\
\boldsymbol{V}^m(x,z) &= \Pi^m(x,+0,z) - \Pi^m(x,-0,z);\\
\boldsymbol{V}^e(x,z) &= \frac{i}{\omega\mu_o}\left[\frac{\partial\Pi^e(x,y=+0,z)}{\partial y} - \frac{\partial\Pi^e(x,y=-0,z)}{\partial y}\right].
\end{aligned} \tag{11}$$

Thus, combination of the relationships (10) differentiated with respect to x and z results in the Poisson equations

$$\Delta\boldsymbol{V}^{e,m}(x,z) = \tilde{\boldsymbol{U}}^{e,m}(x,z) \tag{12}$$

where $\Delta = \frac{\partial^2}{\partial x^2} + \frac{\partial^2}{\partial z^2}$, and $\tilde{\boldsymbol{U}}^{e,m}(x,z)$ are, by definition,

$$\begin{aligned}
\tilde{\boldsymbol{U}}^m(x,z) &= \frac{\partial\tilde{\eta}_x(x,z)}{\partial x} + \frac{\partial\tilde{\eta}_z(x,z)}{\partial z}\\
\tilde{\boldsymbol{U}}^e(x,z) &= \frac{\partial\tilde{\eta}_x(x,z)}{\partial z} - \frac{\partial\tilde{\eta}_z(x,z)}{\partial x}
\end{aligned} \tag{13}$$

After substituting (7) into (11), (12) and performing double Fourier transformation we can readily obtain $a^{e,m}(\alpha,\beta)$

$$a^{e,m}(\alpha,\beta) = -\frac{\boldsymbol{U}^{e,m}(\alpha,\beta)}{\rho^2\varphi_{e,m}(\rho)} \tag{14}$$

where

$$\begin{aligned}
\varphi_{e,m}(\rho) &= \frac{\boldsymbol{P}_0^{e,m}(\rho,y=+0) - \boldsymbol{P}_0^{e,m}(\rho,y=-0)}{\boldsymbol{P}_1^{e,m}(\rho)},\\
\boldsymbol{P}_0^e(\rho,y) &= \frac{\partial\boldsymbol{P}^e(\rho,y)}{\partial y}, \qquad \boldsymbol{P}_0^m(\rho,y) = \boldsymbol{P}^m(\rho,y) * \varepsilon(y),\\
\varepsilon(y) &= \begin{cases}\varepsilon_{xx}^+, & y>0\\ \varepsilon_{xx}^-, & y<0\end{cases}
\end{aligned} \tag{15}$$

$\varepsilon_{xx}^{\pm}$ are related to the dielectric layers interfaced at the plane $y = 0$. Hence the functions $\boldsymbol{U}^{e,m}(\alpha,\beta)$, the double Fourier transforms of $\tilde{\boldsymbol{U}}^{e,m}(x,z)$ defined in (13), can be obtained in an explicit form

$$\begin{aligned}
\boldsymbol{U}^e(\alpha,\beta) &= i\beta\eta_x(\alpha,\beta) - i\alpha\eta_z(\alpha,\beta)\\
\boldsymbol{U}^m(\alpha,\beta) &= i\alpha\eta_x(\alpha,\beta) + i\beta\eta_z(\alpha,\beta)
\end{aligned} \tag{16}$$

It is noteworthy that the meromorphic functions $\varphi_{e,m}(\rho)$ appeared to be same as those in (3). The poles and nulls of $\varphi_{e,m}(\rho)$ correspond to wavenumbers of eigen LSE and LSM modes in the uniform multilayered plane waveguide, which is produced from the original structure (Fig. 1) either by eliminating the patch S (nulls) or by fully metallizing the interface at the plane $y = 0$ (poles).

Thus the relationship (7) accompanied by (14), (16) represents an alternative form of Green's function to relate the potentials $\Pi^{e,m}(x,y,z)$ to the functions $\boldsymbol{U}^{e,m}(\alpha,\beta)$ incorporating the Fourier transforms of surface currents.

Now we proceed to the boundary conditions (4), (5). After substituting (9), (10) into (4) and denoting

$$\boldsymbol{F}^{e,m}(x,z) + \boldsymbol{V}^{e,m}(x,z)/\boldsymbol{Y} = \boldsymbol{W}^{e,m}(x,z) \tag{17}$$

we have

$$\begin{aligned}
\frac{\partial\boldsymbol{W}^e(x,z)}{\partial z} - \frac{\partial\boldsymbol{W}^m(x,z)}{\partial x} &= 0\\
\frac{\partial\boldsymbol{W}^e(x,z)}{\partial x} + \frac{\partial\boldsymbol{W}^m(x,z)}{\partial z} &= 0\\
\{x,z\} \in S,&
\end{aligned} \tag{18}$$

On the other hand, the functions $\boldsymbol{F}^{e,m}(x,z)$, $\boldsymbol{V}^{e,m}(x,z)$ and $\tilde{\eta}_{x,z}(x,z)$ can be represented in the terms of functions $\boldsymbol{U}^{e,m}(\alpha,\beta)$ by making use of (7), (11), (14), and double Fourier transformation of (12). Thus substituting the resultant expressions into (5) and (17) yields the set of dual integral equations

$$\begin{aligned}
-\frac{1}{4\pi^2}\iint_{-\infty}^{+\infty} &\boldsymbol{Q}^{e,m}(\alpha,\beta)\boldsymbol{U}^{e,m}(\alpha,\beta)\\
&\cdot\frac{\exp\{i(\alpha x+\beta z)\}}{\rho^2}\,d\alpha\,d\beta\\
&= \boldsymbol{W}^{e,m}(x,z) + \boldsymbol{W}_i^{e,m}(x,z), \qquad \{x,z\}\in S,
\end{aligned} \tag{19}$$

$$\begin{aligned}
-\frac{1}{4\pi^2}\iint_{-\infty}^{+\infty} &\begin{Bmatrix} i\alpha\boldsymbol{U}^m(\alpha,\beta) + i\beta\boldsymbol{U}^e(\alpha,\beta)\\ i\beta\boldsymbol{U}^m(\alpha,\beta) - i\alpha\boldsymbol{U}^e(\alpha,\beta)\end{Bmatrix}\\
&\cdot\frac{\exp\{i(\alpha x+\beta z)\}}{\rho^2}\,d\alpha\,d\beta = 0, \qquad \{x,z\}\notin S
\end{aligned} \tag{20}$$

where the kernels $\boldsymbol{Q}^{e,m}(\alpha,\beta)$ of (19) are

$$\boldsymbol{Q}^{e,m}(\alpha,\beta) = \left[\frac{1}{\varphi_{e,m}(\rho)} - \frac{1}{Y}\right] \tag{21}$$

the functions $\boldsymbol{W}_i^{e,m}(x,z)$ correspond to incident wave; the functions $\boldsymbol{W}^{e,m}(x,z)$ and $\boldsymbol{U}^{e,m}(\alpha,\beta)$ are to be determined. It is important to emphasize that the functions $\boldsymbol{W}^{e,m}(x,z)$ satisfy the Laplace equation and are coupled by the Cauchy-Riemann relationships (18), resulting immediately from (4).

To conclude the derivation we point out its main features. The principal distinction of developed approach is that it yields a diagonalized set of integral equations (19), (20). Such a formulation enables reduction of the size of the final algebraic system ensuing from the Galerkin routine, even though (19), (20) are coupled by the relationships (18). This advantage is of the utmost significance for analysis of complex structures comprising a number of patches and apertures located at different interfaces of multilayered substrate. In addition, the functions $\varphi_{e,m}(p)$ of the kernel (21) can be evaluated for LSE and LSM modes separately because each of them depends only on the arrangement of substrate but not on the discontinuity shape.

However, a boundary value problem cannot be cast into the form of (18)–(20) for any arbitrary structure. To obtain such a formulation the following necessary conditions must be fulfilled:

1) The fields in the structure are expressible in the terms of pair independent potential functions;

2) Each potential function satisfies individually the homogeneous boundary conditions at the uniform interfaces of subregions, but superposition of the potentials should only be used to meet the piecewise boundary conditions at the discontinue interfaces.

These stipulations constrain a class of the structures to be amenable to treatment with the diagonalized set of equations. In particular, if a substrate contains ferrite slabs or biaxial anisotropic dielectric layers (all three diagonal components of diagonalized tensor $\tilde{\varepsilon}$ are different: $\varepsilon_{xx} \neq \varepsilon_{yy} \neq \varepsilon_{zz}$) the relevant boundary value problem could be put in the form of only integral equations (2) but not (18)–(20).

III. Method of Solution

Galerkin's method in spectral domain lends itself to solving the integral equations (2) or (19), (20). Such a technique is fairly elaborated now and intensively exploited for the analysis of miscellaneous planar structures (see, e.g. [3]–[6], [11], [12], [14]–[24]). Therefore, only the principal aspects of the developed approach are discussed in this paper. Some mathematical details and examples of the sets of basis functions are given in the APPENDIX.

A conventional formulation of the Galerkin procedure pertains only to treating the set (2). But solution of the equations (18)–(20) is somewhat different. In order to illustrate the modified routine, we consider the eigenvalue problem for disk-shaped microstrip resonator on dielectric substrate (Fig. 1, the circular patch S is assumed to be a perfect conductor).

A. Solution for Disk-Shaped Microstrip Resonator

To deal with the problem at hand it is most convenient to make use of cylindrical coordinates $\{r, \vartheta\}$ ($x = r\cos\vartheta$, $z = r\sin\vartheta$). We start with recovering the functions $\boldsymbol{W}^{e,m}(x,z)$ satisfying the Laplace equation and relationships (18). Then, in the case of laterally unbounded structure, we have

$$\begin{aligned} \boldsymbol{W}^{e}(x,z) &= i\omega\mu_0 r^j \exp(ij\vartheta)u_j, \\ \boldsymbol{W}^{m}(x,z) &= -k_0^2 r^j \exp(ij\vartheta)u_j/\varepsilon_0, \qquad j = 0,1\cdots \end{aligned} \tag{22}$$

where j is the number of variations with respect to ϑ-coordinate; constant u_j is as yet undetermined. The respective solutions of integral equations (19), (20) represented in the polar coordinates $\{\rho, \theta\}$ in spectral domain ($\alpha = \rho\cos\theta$, $\beta = \rho\sin\theta$), take the form

$$\begin{Bmatrix} \boldsymbol{U}^m(\alpha,\beta) \\ \boldsymbol{U}^e(\alpha,\beta) \end{Bmatrix} = \begin{Bmatrix} \phi^m(\rho) \\ \phi^e(\rho) \end{Bmatrix} \exp(ij\theta), \qquad j = 0,1,\cdots \tag{23}$$

Substitution of (23) into (19) entails the pair of integral equations

$$\int_{-\infty}^{+\infty} \begin{Bmatrix} -\phi^m(\rho)/k_o^2\varphi_m(\rho) \\ \phi^e(\rho)/\varphi_e(\rho) \end{Bmatrix} \boldsymbol{J}_j(\rho r)/\rho\, d\rho = u_j r^j, \qquad r \leq \boldsymbol{R} \tag{24}$$

where $\boldsymbol{J}_j(\rho r)$ is a Bessel function and $\boldsymbol{R}$ is the radius of S. In accordance with Galerkin's method $\Phi^{e,m}(\rho)$ is expanding in the series of basis functions $\Phi_{jq}^{e,m}(\rho)$ of (A.18)

$$\phi^{e,m}(\rho) = \sum_{q=1}^{\infty} X_{jq}^{e,m}\Phi_{jq}^{e,m}(\rho), \qquad j = 0,1,\cdots, \tag{25}$$

TABLE I

M \ R/h_1	2	6	10
1	12.06160 55.80	4.68220 85.03	2.89056 94.52
2	11.99756 57.08	4.49529 95.79	2.70358 110.9
3	11.99736 57.08	4.49486 95.97	2.70386 110.9
4	11.99736 57.08	4.49486 95.96	2.70386 110.9

and after the standard manipulations in (24) we obtain an infinite system of linear algebraic equations (SLAE)

$$\begin{aligned} \sum_{\substack{q=1 \\ n=0}}^{\infty} X_{nq}^{e} I_{jpnq}^{e} &= j' u_j \delta_{p1}, \\ \sum_{\substack{q=1 \\ n=0}}^{\infty} X_{nq}^{m} I_{jpnq}^{m} &= -k_0^2 u_j \delta_{p1}, \\ p = 1,2,\cdots, \qquad j &= 0,1,\cdots, \end{aligned} \tag{26}$$

where $X_q^{e,m}$ are coefficients to be determined; $j' = j$; and the matrix elements $I_{ipnq}^{e,m}$ take the following form

$$I_{jpnq}^{e,m} = \delta_{nj} \int_{o}^{+\infty} \Phi_{nq}^{e,m}(\rho)\zeta^{e,m}(\rho)\Phi_{jp}^{e,m}(\rho)\, d\rho \tag{27}$$

where δ_{pq} is Kronecker's symbol and $\zeta^{e,m}(\rho) = 1/\rho\varphi_{e,m}(\rho)$.

It is important to note that the SLAE (26) contains an additional unknown coefficient u_j. The lacking equation completing the SLAE (26) is obtained by substituting (23), (25) into (20). It results in a simple coupling relationship

$$(2j+1)X_1^e + X_1^m = 0, \qquad j = 0,1,\cdots. \tag{28}$$

Hence the requirement of consistency of (26) with (28) yields the secular equation for eigen frequencies.

For computations the infinite SLAE (26) is truncated to finite size, and the advantages of the numerical quadrature (A.12) are taken to evaluate the integral (27). The accuracy of these approximations has been extensively explored. The Table I exemplifies an inner convergence of normalized resonance frequency (upper row) and Q-factor due to radiation losses (lower row) versus the number M of basis function retained in (25). The results are presented for the eigenmode with $j = 1$ in the laterally unbounded circular microstrip resonator on dielectric substrate of thickness h_1 and permittivity ε_1 (the distance between resonant patch and the upper covering plate was $h_2 = 10h_1$; $\varepsilon_1 = 9.8$, $\varepsilon_2 = 1$).

It is necessary to note that convergence of the integral (27) in the expression of matrix elements $I_{jpnq}^{e,m}$ had been improved [see (35)] before a numerical quadrature (A.12) was applied. After that a direct summation of not more than 20 terms suffices for the data of Table I to be completely stable.

The above solution needs a slight modification, as a disk-shaped resonator is embedded into the rectangular shielding cavity. Indeed, the boundary conditions at the lateral walls could be fulfilled only by infinite sum of the functions (22) satisfying the Laplace equation and relationships (18). Hence, accounting for the symmetry of the structure (electric and

magnetic walls are placed at the planes $x = 0$ and $z = 0$, respectively. Fig. 1, the functions $\boldsymbol{W}^{e,m}(x,z)$ can be represented in the form of series

$$\boldsymbol{W}^{e}(x,z) = i\omega\mu_0 \sum_{j=0}^{\infty} u_j r^{2j+1} \sin((2j+1)\vartheta);$$
$$\boldsymbol{W}^{m}(x,z) = -k_0^2/\varepsilon_0 \sum_{j=0}^{\infty} u_j r^{2j+1} \cos((2j+1)\vartheta); \quad (29)$$

where j is the number of variations with respect to ϑ-coordinate; coefficients u_j are to be determined. After substituting (29) into (19), (20) we obtain (28) and the SLAE (26), in which $j' = 2j+1$ and the matrix elements take the form

$$I^{e,m}_{jpnq} = \sum_{i,r=o}^{\infty} \nu_i \Phi^{e,m}_{nq}(\rho_{ir}) \zeta^{e,m}(\rho_{ir}) \Phi^{e,m}_{jp}(\rho_{ir}) \quad (30)$$

with

$$\zeta^{\left\{ {e \atop m} \right\}}(\rho_{ir}) = \left\{ {\sin((2n+1)\xi_{ir})\sin((2j+1)\xi_{ir}) \atop \cos((2n+1)\xi_{ir})\cos((2j+1)\xi_{ir})} \right\} \div \rho_{ir}\varphi_{e,m}(\rho_{ir})$$
$$\xi_{ir} = \mathrm{Arctg}(\beta_r/\alpha_i), \qquad \alpha_i = i\pi/L_x,$$
$$\beta_r = (2r+1)\pi/2L_z, \qquad \rho^2_{ir} = \alpha_i^2 + \beta_r^2,$$
$$\nu_i = 1 - \delta_{oi}/2.$$

The tests of inner convergence for the shielded configuration of the resonator have shown that one to three radial and two to three azimuthal basis functions suffice for computational error not to exceed 0.1%.

So, fast convergence behavior of final solutions has been achieved owing to the advanced expansion basis used, along with precise computing the matrix elements for the SLAE (26). Insofar as the principal aspects of choosing the basis functions have already been discussed in the literature (see, e.g. [2]–[10]), we consider only the peculiarities of approximations adopted in this paper.

B. Basis Functions

In line with Galerkin's method, $\eta_{x,z}(\alpha,\beta)$ of (2) or $\boldsymbol{U}^{e,m}(\alpha,\beta)$ of (19) are expanded into the series of basis functions $\boldsymbol{u}^{e,m}_{jq}(\alpha,\beta)$

$$\left\{ {\eta_{x,z}(\alpha,\beta) \atop \boldsymbol{U}^{e,m}(\alpha,\beta)} \right\} = \sum_{j,q=1}^{\infty} \boldsymbol{X}^{e,m}_{jq} \boldsymbol{u}^{e,m}_{jq}(\alpha,\beta) \quad (31)$$

where coefficients $\boldsymbol{X}^{e,m}_{jq}$ are undetermined yet. Substituting (31) into (2) or (19) yields the infinite SLAE with matrix elements expressed in the form of double infinite integrals.

$$I^{e,m}_{npjq} = -\frac{1}{4\pi^2} \iint_{-\infty}^{+\infty} \boldsymbol{u}^{e,m}_{np}(\alpha,\beta)\zeta(\alpha,\beta)\boldsymbol{u}^{e,m}_{jq}(\alpha,\beta)\, d\alpha\, d\beta, \quad (32)$$

where $\zeta(\alpha,\beta)$ denotes either $\boldsymbol{Q}^{e,m}(\alpha,\beta)$ of (19) or any component of $\hat{G}(\alpha,\beta)$ of (2).

In order to obtain a uniform and rapid convergence of numerical procedure, we make use of the complete sets of basis functions (Appendix C), orthonormalized in space domain with respect to the weight factor. This factor is introduced to account explicitly for the behavior of the electrostatic field in the vicinity of the discontinuity edges. The advanced expansion bases have been devised for areas S of several specific shapes such as rectangle, parallelogram, and ellipse. For S of arbitrary shape the basis functions incorporating the weighted Chebyshev polynomials with spline functions in space domain have proved to be of high efficiency. Besides, to solve the integral equations (2), (19), (20) for the fields on apertures, the advantage of Schwinger's transformation [25] has been taken in the expansion bases (Appendix A). Note that appropriate bases could be defined in both space and spectral domain, whereas the use of an analytical form of basis functions is made only in spectral domain to calculate the double integrals for $\boldsymbol{I}^{e,m}_{npjq}$ in (32).

C. Evaluation of the Matrix Elements

A precision of calculations of the matrix element $\boldsymbol{I}^{e,m}_{npjq}$ has shown in Appendix A affects substantially the convergence and accuracy of final solutions. This important aspect has been largely neglected in the available publications. To address this problem we discuss here the computational problems of the developed technique.

Matrix element $\boldsymbol{I}^{e,m}_{npjq}$ is represented in (32) by the double infinite integral. Its integrand may contain the number of poles located on and nearby the path of integration. Treatment of such integrals faces two challenges: i) correct calculation of the pole contributions [12], [13], [15] and ii) evaluation of a slow convergent infinite integral. To compute the value of such singular integrals the efficient numerical quadrature have been devised.

If the structure to be dealt with is boundless with respect to both x- and z- direction, it is expedient to represent (32) in the polar coordinates (ρ,θ). Then the integration in spectral domain can be merged into a summation by making use of the numerical quadrature such as (A.12) (see Appendix B)

$$\boldsymbol{I}^{e,m}_{npjq} \simeq \sum_{k=1}^{K} \left(i\pi^2 \sum_{r=1}^{Np} \mathrm{res}\, f(\rho_{rk},\theta_k) \cdot (\mathrm{sign}(\mathrm{Im}\,\rho_{rk}) + itg(\pi\rho_{rk})) + \sum_{r=1}^{\infty} \boldsymbol{f}(y_r,\theta_k) \right), \quad (33)$$

where $\boldsymbol{f}(\rho,\theta) = \boldsymbol{u}^{e,m}_{np}(\rho,\theta)\zeta(\rho,\theta)\boldsymbol{u}^{e,m}_{jq}(\rho,\theta)$, $y_r = (\boldsymbol{r} - 1/2)\,\pi/L$, and L is a sampling scale; N_p is the number of poles located on and nearby the real axis of complex plane ρ; K is the number of nodes for a numerical integration over θ-coordinate.

Another approximation of $\boldsymbol{I}^{e,m}_{npjq}$ should be used if the structure of Fig. 1 is confined by plate-parallel screens at the planes $x = \pm\boldsymbol{L}_x$ (e.g., for discontinuity of finline embedded into rectangular waveguide housing composed of the covering plate above and a conductive backing beneath the substrate, and the lateral walls at the planes $x = \pm\boldsymbol{L}_x$). In this case, the boundary conditions at the lateral walls entail merging the integration with respect to α into a summation [see (1)].

The other integration in (32) is amenable to the numerical quadrature (A.12). Thus

$$I^{e,m}_{npjq} \simeq \sum_{k=-\infty}^{\infty} \left(i\pi \sum_{r=1}^{P_k} \operatorname{res} f(\alpha_k, \beta_{rk}) (\operatorname{sign}(\operatorname{Im} \beta_{rk}) + itg(\pi\beta_{rk})) + \sum_{r=-\infty}^{\infty} f(\alpha_k, z_r) \right), \quad (34)$$

where $f(\alpha,\beta) = u^{e,m}_{np}(\alpha,\beta)\zeta(\alpha,\beta)u^{e,m}_{jq}(\alpha,\beta)$; $\alpha_k = k\pi/L_x$; $z_r = (r-1/2)\pi/L_z$ and L_z is a sampling scale; P_k is the number of poles of $\zeta(\alpha,\beta)$ located on and near the real axis β. These poles correspond to the eigenmodes which have k variations of field with respect to the x-coordinate in a partially loaded rectangular waveguide. When the frequency runs below the waveguide cutoff, no traveling wave exists and $P_k = 0$ for any k.

For the problem of the discontinuity inserted into a shielding cavity, $I^{e,m}_{npjq}$ takes the same form of double sum (34) with $P_k = 0$. Such a formulation ensues immediately from the boundary conditions at the lateral walls or can be obtained from (32) by formally merging both integrations into summations in accordance with (1). However, we have to note that (34) represents an exact expression of $I^{e,m}_{npjq}$ only if the structure contains the dielectric layers. As a substrate has a ferrite layer, the boundary conditions at the lateral walls of shielding box are altered and (1) ceases to hold. Nevertheless, the formulation (34) has proved to remain a very good approximation for $I^{e,m}_{npjq}$ in any case [14].

D. Improvement of Convergence in the Series (33), (34)

An accurate calculation of the series in (33), (34) used to be based on various numerical approximations and requires an individual treatment for any particular set of basis functions. Nevertheless, for all the expansion bases presented in Appendix C, both single (33) and double (34) series can be effectively evaluated after improvement of their convergence behavior.

The series in (33) as well as in (A.12) implicate a single infinite summation only. In order to refine their convergence behavior we have extracted a uniform asymptotic form of $f(\rho,\theta)$ as $\rho_r \Rightarrow \infty$ for any θ. The series of difference elements remaining in (33) after subtracting the asymptotic terms converges fairly rapidly. Therefore, it can be truncated after direct summation of the finite number N of elements. A contribution of the slowly converging series of asymptotic terms can be precisely calculated. To evaluate it, the latter summation is merged backward into an integration, which results in analytical quadrature [5].

Note that such a rearrangement of the series (33) corresponds to immediately extracting an asymptotic form of integrand in (32) and making use of the numerical quadrature (33) only for evaluation of the rapidly converging integral of a difference integrand.

To illustrate the above routine, we consider the matrix elements (27) for the problem of a disk-shaped microstrip resonator. Since $\varphi^{\{e\atop m\}}(\rho) \Rightarrow c^{\{e\atop m\}}\rho^{\pm 1}$ as $\rho \Rightarrow \infty$, we handle the integral as follows:

$$I^{e,m}_{jpjq} = \int_0^{+\infty} J_{2p+j-1/2}(\rho r) J_{2q+j-1/2}(\rho r) \cdot \rho^{\pm 1}/\varphi^{\{e\atop m\}}(\rho)\frac{d\rho}{\rho} = \int_0^{+\infty} J_{2p+j-1/2}(\rho r) J_{2q+j-1/2}(\rho r) \cdot \left(\frac{\rho^{\pm 1}}{\varphi^{\{e\atop m\}}(\rho)} - \frac{1}{c^{\{e\atop m\}}} \right) \frac{d\rho}{\rho} + \frac{\delta_{pq}}{2(2p+j-1/2)c^{\{e\atop m\}}} \quad (35)$$

The integral remaining on the right-hand side (35) is amenable to the numerical quadrature (33). The series resulting from (33) converges rapidly and can be truncated after summation of N terms (here it appeared to suffice $N \leq 20$, see text discussing Table I).

The formulation (34) for shielded structures contains double infinite sum. Because uniform asymptotic form of $f(\alpha,\beta)$ could not be found for both of the arguments simultaneously as $|\alpha|, |\beta| \Rightarrow \infty$, convergence of the series (34) is improved in several steps [8]. At first the finite number of terms is directly summed over both indexes while $|k|, |r| \leq N$. Then, for $|k| > N$ and $|r| \leq N$ the function $f(\alpha,\beta)$ is replaced by its asymptotic form as $\alpha \Rightarrow \infty$ and an infinite sum over k is approximated by the integral. This integral is evaluated in an analytical form like the above single integral for (33). The sum over r as $|r| > N$ and $|k| \leq N$ is handled similarly. At last, the summation of the remaining double infinite sum over both $|k|, |r| > N$ is merged into an integration. The latter integral over an asymptotic form of $f(\alpha,\beta)$ handled in polar coordinates results in an analytical quadrature as well [8].

E. Tests of Convergence

Inner convergence of the final solutions has been thoroughly examined for every particular structure under investigation. The effect of the numbers M_j, M_q of basis functions retained in the expansion (31) and the number N of terms summed in the series (33), (34) of the matrix elements $I^{e,m}_{npjq}$ have been explored.

The Tables II and III exemplify the inner convergence of the solutions for resonance frequency f_r of E-plane fin embedded into the rectangular waveguide housing. Computations have been performed for the same parameters of the structure as in [26]: the waveguide cross-section–$3.098 * 1.549$ mm^2; fin—length = 0.8 mm and height = 1.2 mm; thicknesses of the layers—$h_1 = 0.127$ mm, $h_2 = 1.422$ mm, $h_3 = 1.549$ mm, and permittivities—$\varepsilon_1 = 2.2$, $\varepsilon_2 = \varepsilon_3 = 1$ [numeration of the layers is of Fig. 2(a)]. The results of our computations demonstrate a good agreement with [26].

Thus Tables I–III show that the basis functions (A.13), (A.17), (A.18), and numerical quadratures (33), (34) with improved convergence of the series ensure the computational inaccuracy to be less than 0.1% when $N \leq 20$ and two to three terms with respect to each index are held in the expansion (31).

TABLE II
$M_j = M_q = 2$

N	5	10	15	20	50	[17]
f_r, GHz	34.858	34.973	34.966	34.975	34.977	34.58

TABLE III
$N = 20$

M_j \ M_q	1	2	3
1	35.252	35.128	35.115
2	35.127	34.975	34.966
3	35.119	34.964	34.955

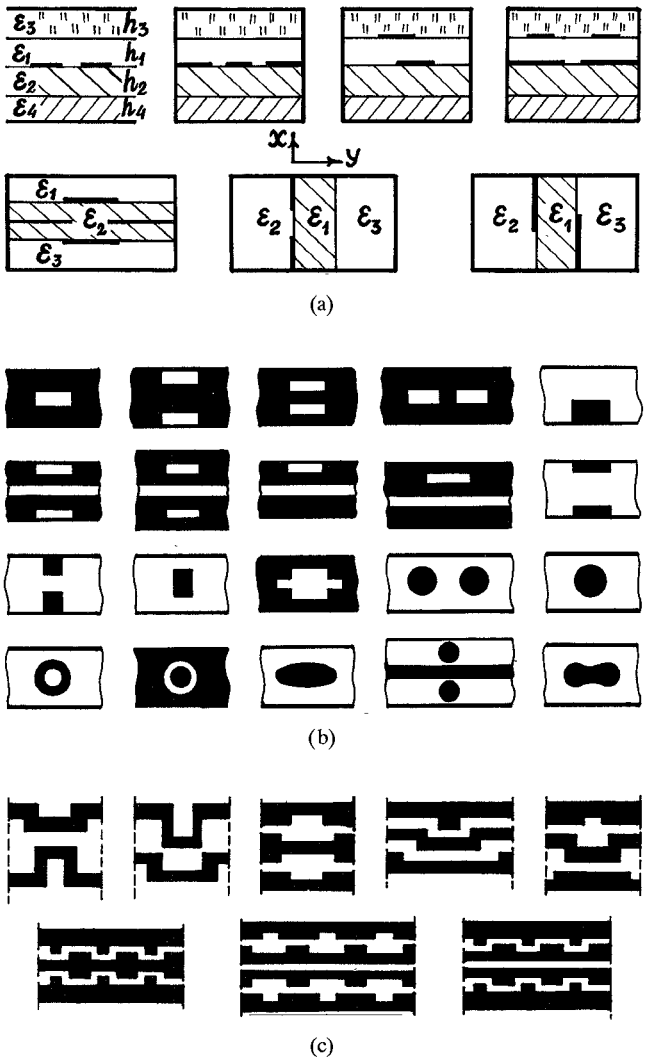

Fig. 2. Cross sections (a) and fragments of plans for resonant (b) and periodic (c) three-dimensional planar structures. Black and whitened parts of the drawings in (b) and (c) correspond to configurations of conductors and demetallized portions of substrate surface, respectively.

IV. Analysis of Planar Resonators and Discontinuities

The developed approach has been applied to analysis of planar and volume transmission lines, resonators, and discontinuities. Their basic configurations (Fig. 2) are listed below:

- Open and shielded, isolated and coupled microstrip, finline and slot resonators (the resonant patches can be of rectangle, disk, ring, ellipse, parallelogram, cross, or arbitrary shape) [8], [17], [18]
- Planar resonators coupled with uniform microstrip or finline (resonant patches and uniform line could be placed either on the same or on other interfaces of multilayered substrate)
- Isolated and coupled finline and microstrip resonators on tangentially magnetized ferrite-dielectric substrate [19]
- Finite set of conductive strips on magnetized ferrite-dielectric substrate inserted into E-plane of rectangular waveguide [20]
- Resonant planar discontinuities embedded into the cross or longitudinal section of rectangular waveguide: apertures and patches of both a specific (rectangular, parallelogram, disk, ring, ellipse, cross, etc.) and arbitrary shapes [18], [21]
- Isolated and periodic discontinuities in planar transmission lines: opened- and shorted-end of microstrip or slot lines, stubs, notches, and meanders in slot and microstrip lines, and so on [22]
- Rectangular waveguides and resonant cavities coupled via the holes in a common wall [23]

Analysis of the aforementioned structures gives rise to either an eigenvalue problem for resonant configurations or a diffraction problem for discontinuities. In the meantime, the scattering matrix for most of the discontinuities in the structures with negligible radiation losses can be recovered from the solutions of the eigenvalue problem instead of the diffraction one. In particular, such an approach has been adapted in [24] to analysis of discontinuities in finlines. Since most of our practical endeavors are directed toward finding eigenfrequencies of resonators or equivalent circuits of discontinuities, the computed results are largely presented for resonant structures.

A. Planar Resonators Coupled with Uniform Planar Line

Let the coupled planar transmission line and resonator be placed on a same surface of dielectric substrate [the plans of several such configurations are shown in Fig. 2(b). The relevant eigenvalue problem gives rise to diagonalized set of homogeneous integral equations (19), (20) where S incorporates two sub-areas: resonant patch (S_1) and segment of uniform line (S_2). The scattering matrix of this discontinuity is recovered from analysis of shielded configuration (rectangular shielding box is formed by electric or magnetic walls located far away from S_1).

The principal feature of our solution is the use of the substantially different sets of basis functions on each subregion. Namely, the expansion basis adopted for an isolated resonator is taken for S_1. But for S_2 the basis functions are composed

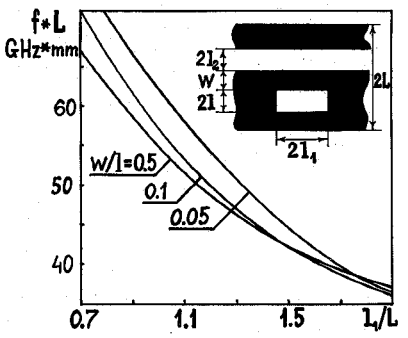

Fig. 3. Resonance frequencies f of fundamental mode in rectangular slot resonator of the aperture $2l * 2l_1$ coupled with uniform finline of the slotwidth $2l_2$ inserted in the waveguide housing of cross-section $4L * 2L$. Black and whitened parts in the fragment of plan correspond to configurations of conductive fins and demetallized apertures on the surface of dielectric substrate of thickness $h_1 = 0.2\ L$, $\varepsilon_1 = 2.2$, $1 = 1_2 = 0.1\ L$.

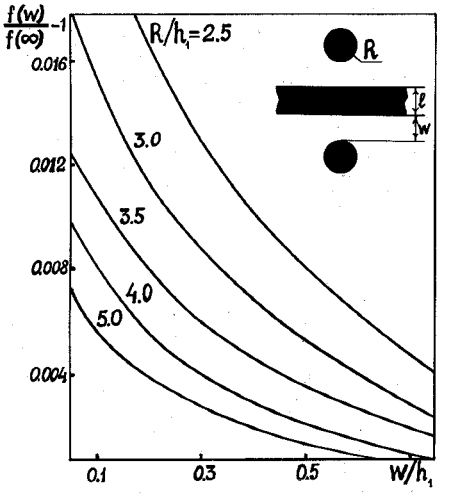

Fig. 4. Normalized resonance frequencies of disk-shaped microstrip resonators coupled with uniform microstrip line of width $l = h_1$ on the grounded dielectric substrate of thickness h_1; $\varepsilon_1 = 9.8$.

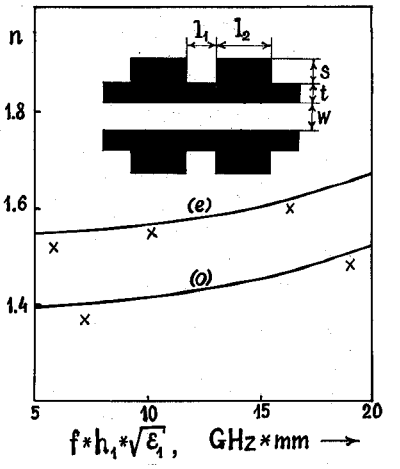

Fig. 5. Delay ratio (n) of even (e) and odd (o) modes as compared with the data of measurements (crosses) for periodically stubbed edge-coupled strip lines. $1_1 = 0.35\ h_1$; $1_2 = 0.196\ h_1$; $w = 0.5\ h_1$; $t = 0.315\ h_1$; $s = 1.9\ h_1$; $h_1 = h_2$; $\varepsilon_1 = \varepsilon_2 = 1.067$; $h_3 = h_4 = 0$.

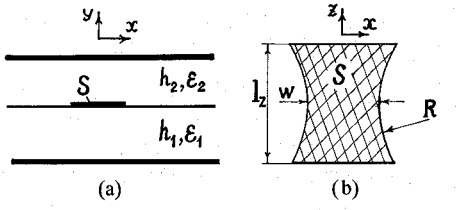

Fig. 6. Shielded microstrip resonator of complex shape: (a) cross section; (b) configuration of resonant conductive patch. $h_1 = 23.4$ mm, $h_2 = 20.6$ mm, $R = 60$ mm, $w = 40$ mm, $1_z = 100$ mm, $\varepsilon_1 = \varepsilon_2 = 1.069$.

of product of sinusoidal functions in the longitudinal coordinate (along the uniform line) and the weighted Chebyshev polynomials of the first kind in the transverse coordinate.

The advantages of expansion bases (A.13) are taken for S_1 in the shape of a rectangle aperture and (A.18) for S_1 in disk-shaped patches. The numerical tests have proved that the solutions for coupled resonators have the same inner convergence as for an isolated disk resonator and rectangular E-plane fin (Tables I–III).

The computed charts of eigenfrequencies for a rectangular slot resonator coupled with finline and a pair of disk-shaped microstrip resonators coupled with microstrip line are shown in Figs. 3 and 4.

B. Periodic Discontinuities in Planar Transmission Lines; Microstrip Resonators of Arbitrary Shape

Periodic discontinuities at the edges of planar conductors [Fig. 2(c)] are widely used as matching, adjusting, and filtering elements of planar circuits. Therefore, accuracy of modeling such structures is of the utmost significance to design complex MIC.

An appropriate boundary value problem has been cast in the form of the set of equations (2) or (18)–(20). Besides, owing to the periodicity of the structure and in compliance with Flocke's theorem, the integral equations are converted into summator ones. Hence, the above technique adopted for analysis of shielded configurations has appeared to be applicable to these problems.

The basis functions (A.20) for the areas S of arbitrary shape have been adopted here. The tests of inner convergence have shown that two to four terms in index j (weighted Chebyshev's polynomials) and four to six terms in index q (spline functions) retained in the expansion (31) provide for a computational error not to exceed 0.5%.

The characteristics computed for edge-coupled strip lines with periodic stubs at the outer edges of strips are presented in comparison with the results of measurements in Fig. 5.

The same routine is applied to simulation of shielded microstrip resonators of arbitrary shape. The computed eigenfrequencies (in gigahertz) as compared with the results of measurements are presented in Table IV for the first two lowest modes in the microstrip resonator of complex shape (Fig. 6). The contour of the conductive patch S is composed of a pair of parallel lines and a pair of circular arcs of radius R [Fig. 6(b)]. The computed results were found to be in a good agreement with experimental data for both structures.

TABLE IV

n	1	2
Calculation	1.021	1.667
Measurement	1.024	1.675

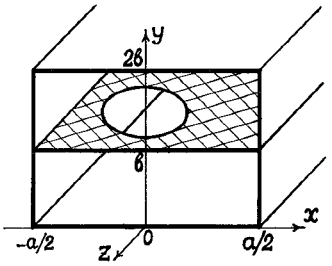

Fig. 7.

C. Coupled Rectangular Waveguides

The analysis of rectangular waveguides coupled through the holes in a common wall is usually based on the Bethe theory for small apertures [27]. To our knowledge the rigorous approach to these problems has been developed only for a few specific configurations [28]–[30]. Meanwhile, the technique presented in the previous sections can be readily adapted to a full-wave solution of waveguide diffraction problems [23].

Let the pair of rectangular waveguides be coupled by the hole S in a common wall of infinitesimal thickness (Fig. 7) and H_{10} or H_{01} mode is assumed incident from $z = \infty$. The relevant boundary value problem can be put in the form of the set of equations such as (18)–(20), where double integration in (19), (20) is replaced by the mixed integro-summator operator. Such a formulation results from the boundary conditions at the lateral waveguide walls, which entail merging the integration with respect to α into a summation [see (1)].

The accuracy of numerical solutions has been examined for the circular hole centered in the midpoint of a wide wall. The tests have demonstrated the same inner convergence of results as in the case of a shielded disk-shaped microstrip resonator (Section III-A).

The computed charts as compared with the data of dipole theory [27] are presented in Fig. 8 to exemplify the effects of increasing the hole size, a/b ratio ($a > b$), and frequency on the dependence of coupling coefficient C versus radius $\boldsymbol{R}$ of a circular aperture.

V. Application to Volume Dielectric Resonators and Discontinuities

Rigorous analysis of MIC with limited dielectric substrates, dielectric resonators (DR), and discontinuities in dielectric waveguides gives rise to more complex boundary value problems than those occurring for planar structures. Nevertheless, the above technique can be effectively applied to simulation of volume configurations if they contain "thin" dielectric discontinuities or DR's (the thickness of irregular layers should be less than both a wavelength and the other sizes of the structure). To address these problems we have devised the approximation of quasi-planar (QP) model. The model is

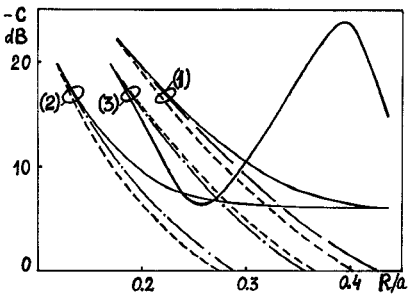

Fig. 8. Coupling coefficient C of rectangular waveguides coupled by a hole in a wide wall: rigorous theory (solid lines) and dipole theory [27] (dashed and dotted lines, which correspond to the data of dipole theory accounting for the effects of the waveguide opposite walls and frequency dependent polarization coefficients, respectively): (1) $b/a = 0.5$, $f * a = 200$ GHz * mm; (2) $b/a = 0.1$, $f*a = 200$ GHz * mm; (3) $b/a = 0.5$, $f*a = 280$ GHz * mm.

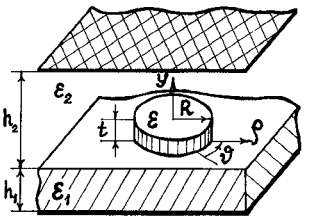

Fig. 9.

substantially based on the bilateral boundary conditions (BCs) that permit replacement of a "thin" dielectric layer by an impedance surface of infinitesimal thickness [31]. Thus the original volume discontinuity structure can be converted into a planar one to be amenable to the developed technique.

A. Disk-Shaped DR

To gain insight into approximations inherent to the QP model we consider the eigenvalue problem for a disk-shaped DR on the unbounded grounded dielectric substrate (Fig. 9). It is assumed that DR has a permittivity ε, $\varepsilon \gg 1$, and its radius $\boldsymbol{R}$ is much more than its thickness t. Under the stipulation $k_0\sqrt{\varepsilon}\,t < 1$, the thick DR can be reduced to infinitesimally thin impedance patch placed at the plane $y = 0$ (Fig. 9). Then the tangential electric $\vec{\boldsymbol{E}}_t$ and magnetic $\vec{\boldsymbol{H}}_t$ fields meet the following BC's at $y = 0$

$$\begin{aligned} \vec{\boldsymbol{H}}_t^+ - \vec{\boldsymbol{H}}_t^- &= \boldsymbol{Y}\vec{\boldsymbol{E}}_t, \qquad r \le R \\ \vec{\boldsymbol{H}}_t^+ &= \vec{\boldsymbol{H}}_t^-, \qquad r \ge R \\ \vec{\boldsymbol{E}}_t^+ &= \vec{\boldsymbol{E}}_t^- = \vec{\boldsymbol{E}}_t, \qquad r < \infty \end{aligned} \tag{36}$$

where $\vec{\boldsymbol{H}}_t^{\pm} = \vec{\boldsymbol{H}}_t^{\pm}(r, \vartheta, y = \pm 0)$ and surface admittance Y takes the form $\boldsymbol{Y} = i\boldsymbol{k}_0\delta/\boldsymbol{Z}_0$, with $\boldsymbol{k}_0$ and $\boldsymbol{Z}_0$-free-space wavenumber and impedance, respectively. The parameter δ for disk-shaped DR is put in the form

$$\delta = 2k_1 \sin(\boldsymbol{k}_1 t/2)/\boldsymbol{k}_0^2 - t\,, \tag{37}$$

where $\boldsymbol{k}_1 = \sqrt{\boldsymbol{k}_0^2\varepsilon - \boldsymbol{k}_t^2}$, $\boldsymbol{k}_t = \gamma_j/\boldsymbol{R}$ with γ_j satisfying the equation $J_j'(\gamma_j) = 0$, $J_j(\gamma)$-Bessel function; $\boldsymbol{k}_t$ is to account approximately for the radial variation of the field. Note that the parameter δ tends to its extreme magnitude of [31] as $\boldsymbol{k}_1 t \ll 1$ and $\boldsymbol{k}_t \Rightarrow 0$.

TABLE V

j	0	3	4	5	8
[32]	11,46	14,12	15,52	16,69	19,95
QP model k_t=0	11,40	14,07	15,17	16,21	19,12
QP model k_t>0	11,65	14,29	15,53	16,72	20,11

The boundary value problem associated with the QP model of disk-shaped DR (BC's (36) are imposed at the plane $y = 0$) gives rise to the set of equations (18)–(20). They can be treated like the case of a perfect conductive patch (Section III). The sole distinction is associated with the value of parameter τ occurring in the basis functions (A.17), (A.18). When we dealt with a perfect conductor, $\tau = 0$ but for the impedance patch, τ has been varied within the range $0 < \tau \leq 1/2$, in order to gain the best convergence of final solutions. The numerical experiments have shown the fastest convergence behavior for eigenfrequencies of fundamental $(j = 0)$ and higher order $(j \neq 0)$ modes when $\tau = 0.5$ and $\tau \approx 0.3$, respectively. Then three to four terms were sufficient to hold in expansion (25) for computational error to be less than 0.1%.

It is important to emphasize that BC's (36) have been derived for the laterally unbounded dielectric layer. Therefore their applicability to the patch formed by limited dielectric layer had to be verified. In order to examine an inaccuracy ensuing from the approximate BC's, the dispersion characteristics of strip dielectric waveguides (DW) calculated on the base of BC's (36) was compared to the results of rigorous analysis [32]. The discrepancy was found to be less than 0.5% across a wide frequency range. The same precision of the QP model demonstrates the Table V for disk-shaped DR. The resonance frequencies (in gigahertz) computed for five eigenmodes are presented in comparison with the results of rigorous analysis [33] for the following parameters of the structure in Fig. 9: $\varepsilon_1 = 9.8$, $\varepsilon = 200$, $h_1 = 1$ mm, $h_2 = 2$ mm, $t = 0.15$ mm, $R = 5$ mm.

The extensive numerical tests have proved the QP model maintains high accuracy of evaluating the integral characteristics such as propagation constants and eigenfrequencies but reduces considerably the time of computations. Duration of calculations with QP model used to be less by an order of magnitude as compared to rigorous analysis in [32], [33].

Figure 10 exemplifies the charts of normalized resonance frequencies f computed for the six lowest eigenmodes in disc DR on dielectric substrate versus the impedance parameter δ. Since the higher order modes with $j \geq 1$ had the radiation losses the curves were broken as Q-factor had become less than 100.

B. Microstrip Resonator on Substrate of Finite Length

In practice the planar structures used to be of finite lateral extent and contain limited dielectric substrates. The QP model has proved to be a very convenient tool for simulation of the effects associated with the substrate of finite size. In particular, it has been applied to analysis of rectangular microstrip resonator on dielectric substrate of finite length (L_s) suspended in the waveguide housing (Fig. 11). Table VI

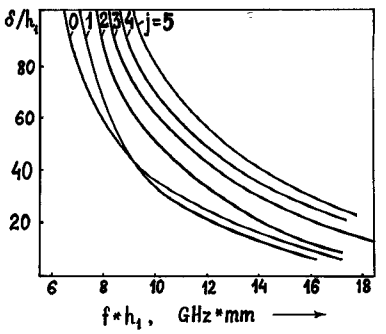

Fig. 10. Normalized resonance frequencies of six lowest eigenmodes in an isolated disk dielectric resonator of radius R on dielectric substrate, $R = h_2 = 5h_1$, $\varepsilon_1 = 9.8$, $\varepsilon_2 = 1$.

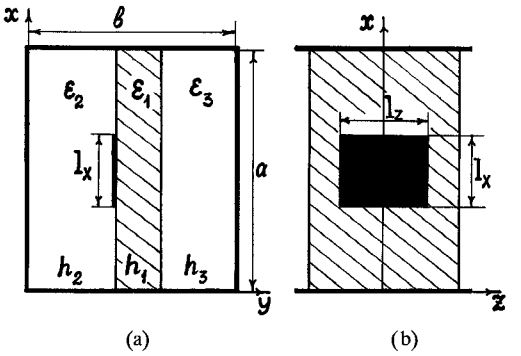

Fig. 11. Cross section (a) and plan (b) of a rectangular microstrip resonator of on the suspended dielectric substrate of finite length L_s. A rectangular conductive patch in plan is darkened.

TABLE VI

L_s, mm	0(r)	0,7	3,0	5,0	5,5	6,5	∞	∞(r)
f, GHz	27.23	27.22	26.99	26.28	25.97	25.49	25.43	25.03

displays shift of the eigen frequency f of fundamental mode versus L_s. The results obtained in the frame QP model are compared to the data of rigorous calculations for the extreme cases of an infinite $(L_s = \infty)$ and a vanishing $(L_s = 0)$ substrate length. These two columns has the mark (r). The parameters of the structure were as follows: $h_1 = 0.127$ mm, $h_2 = h_3 = 0.711$ mm, $\varepsilon_2 = 1$, $\varepsilon_1 = 2.2$, $1_x = 1$ mm, $1_z = 5$ mm, $a * b = 3.098 * 1.549$ mm^2.

VI. Conclusions

The developed numerical-analytical approach enables to extend substantially the class of three-dimensional planar and waveguide problems to be amenable to rigorous analysis. It has been applied to simulation of complex planar and waveguide microwave circuits. The efficiency and flexibility of the technique is exemplified by the numerical results for several structures containing dielectric loading. The frame of this paper did not allow us to discuss the features of the technique in the case of gypotropic, in particular, ferrite loading. We expect it to be the topic of another our publication.

Appendix

A. Qualitative foundation for a numerical solution of dual integral or summator equations like (2), (19), (20) originates

from the theory of one-dimensional integral and integro-differential operators [34]. Let us consider the following equations in a space domain

$$\Psi \boldsymbol{f} = \left\{ \begin{array}{c} 1 \\ \frac{d^2}{dx^2} \end{array} \right\} \int_a^b \boldsymbol{f}(x')\boldsymbol{g}(x,x')\,dx' = \boldsymbol{f}_0(x), \qquad x \in [a,b] \tag{A.1}$$

where Ψ is a linear integral or integro-differential operator; $\boldsymbol{f}(x)$ is the function to be determined, and $\boldsymbol{f}_0(x)$ is determined. A kernel of operator Ψ is known to have a logarithm singularity for any electrostatic or electrodynamic two-dimensional problem. Then such a singularity of $\boldsymbol{g}(x,x')$ can be explicitly extracted

$$\boldsymbol{g}(x,x') = \boldsymbol{g}_0(x,x') + \boldsymbol{g}_1(x,x'), \tag{A.2}$$

where $\boldsymbol{g}_0(x,x') \sim \ln|t(x) - t(x')|$ as $x \Rightarrow x'$, and a function $\boldsymbol{g}_1(x,x')$ is regular for any $x, x' \in [a,b]$. The function $t(x)$ introduces a new variable, which ranges from -1 to $+1$ so that $|t(a)| = |t(b)| = 1$. For the problems associated with the fields on the aperture, $t(x)$ takes the form of Schwinger's transformation [25], but $t(x)$ is a plain linear function for the problems of patches.

To solve (A.1), $\boldsymbol{f}(x)$ can be put in the form of series of the weighted functions $\tilde{\boldsymbol{u}}_j(x)$ which compose a complete set of eigen functions for the operator Ψ with the kernel $\boldsymbol{g}_0(x,x')$

$$\boldsymbol{f}(x) = \sum_{j=1}^{\infty} X_j \frac{\tilde{\boldsymbol{u}}_j(x)t'(x)}{\lambda_j N_j \sqrt{1-[t(x)]^2}} \tag{A.3}$$

where coefficients X_j are as yet undetermined; $\tilde{\boldsymbol{u}}_j(x)$ takes the form of Chebyshev's polynomials of the first—$T_{j-1}(t(x))$ or second—$\boldsymbol{U}_{j-1}(t(x))$ kind for Ψ to be an integral or integro-differential operator, respectively; the norm N_j and eigen value λ_j related to $\tilde{\boldsymbol{u}}_j(x)$ are defined as follows

$$\begin{aligned} &\int_a^b \frac{\tilde{\boldsymbol{u}}_j(x')\boldsymbol{g}_0(x,x')}{\sqrt{1-[t(x')]^2}}\,dx' = \lambda_j \tilde{\boldsymbol{u}}_j(x); \\ &\int_a^b \frac{\tilde{\boldsymbol{u}}_j(x')\tilde{\boldsymbol{u}}_m(x')}{\sqrt{1-[t(x')]^2}}\,dx' = \begin{cases} N_j, & m = j \\ 0, & m \neq j \end{cases} \end{aligned} \tag{A.4}$$

Substituting (A.2), (A.3) into (A.1) and making use of the orthogonality condition (A.4) result in the infinite system of linear algebraic equations (SLAE):

$$X_m + \sum_{j=1}^{\infty} q_{mj}^1 X_j = X_m^0 \tag{A.5}$$

where X_m^0 is a convolution of $\boldsymbol{f}^0(x)$ with the weighted function $\tilde{\boldsymbol{u}}_m(x)$; and $\boldsymbol{q}_{mj}^1$ takes the form

$$\boldsymbol{q}_{mj}^1 = \int_a^b \frac{\tilde{\boldsymbol{u}}_m(x)}{\sqrt{1-[t(x)]^2}}\,dx \int_a^b \frac{\tilde{\boldsymbol{u}}_j(x')\boldsymbol{g}_1(x,x')}{\sqrt{1-[t(x')]^2}}\,dx'. \tag{A.6}$$

The SLAE (A.5) is remarkable in that it is well-conditioned quasi-regular system that can be truncated to finite size. Such a finite SLAE provides uniform convergence of its solutions while increasing the number of terms in the expansion (A.3).

In the particular case of $\boldsymbol{g}_1(x,x')$, represented by a finite sum of terms like $\tilde{\boldsymbol{u}}_j(x') * \tilde{\boldsymbol{u}}_m(x)$, the series (A.3) is reduced to a finite sum producing an exact solution of (A.1).

In a general case $\boldsymbol{g}(x,x')$, the kernel of (A.1), can be cast in the form of an Fourier transformation (integral or discrete). Then Galerkin's procedure with expansion basis (A.3) applied immediately to (A.1) yields the SLAE like (A.5). Its matrix elements $\boldsymbol{q}_{m,j}$ are the most convenient for further manipulations to express in spectral domain

$$\boldsymbol{q}_{mj} = \int_{-\infty}^{+\infty} \boldsymbol{u}_m(\alpha)G(\alpha)\boldsymbol{u}_j(\alpha) \tag{A.7}$$

where $G(\alpha)$ is the Fourier transform of $\boldsymbol{g}(x,x')$ and

$$\boldsymbol{u}_m(\alpha) = \int_a^b \frac{\tilde{\boldsymbol{u}}_m(x)t'(x)\exp\{i\alpha x\}}{\sqrt{1-[t(x)]^2}}\,dx. \tag{A.8}$$

It is necessary to emphasize that the SLAE with the matrix elements (A.7) could be rearranged to the form (A.5) by extracting the explicit asymptotic form of $\boldsymbol{G}(\alpha)$ as $|\alpha| \Rightarrow \infty$ and evaluating the integral of it in an analytical form. A parity of the latter SLAE and (A.5) follows immediately from definitive relation of the asymptotic behavior of $\boldsymbol{G}(\alpha)$ as $|\alpha| \Rightarrow \infty$ to $\boldsymbol{g}_0(x,x')$ as $x \Rightarrow x'$.

Hence, we can conclude that both an appropriate choice of basis functions $\boldsymbol{u}_m(\alpha)$ and a proper approximation of the slow convergent integrals in (A.7) have the same effect on the accuracy of Galerkin's method in spectral domain.

The weighted Chebyshev's polynomials are the most pertinent expansion basis to the problems associated with thin perfect conductors. Being the eigen functions of operator Ψ with kernel $\boldsymbol{g}_0(x,x')$, they also fulfill exactly the edge condition. Such a basis could be applied to the treatment of the structures with any edge singularity. However, the weighted Gegenbauer polynomials accounting for the proper edge condition have proved to maintain a better convergence behavior of final solutions [5], [32], [33], [35], [36].

B. In order to evaluate the integrals like (A.7) we make use of a numerical quadrature. Such an approximation is suitable for integration of smooth regular functions. However, the integrand in (A.7) contains the number of poles related to the singularities of $\boldsymbol{G}(\alpha)$. They are located on and near the path of integration. To avoid this difficulty the authors of [12], [13] have proposed to remove formally the singularities from the contour of integration. But such an analytical artifice might refine an accuracy of approximation only if the sampling scale in numerical quadrature were much less than a distance from a pole to the path of integration. To eliminate such a restriction we have devised the uniform numerical quadrature adapted for evaluating infinite singular integrals.

Let us consider an infinite converging integral over real axis

$$\boldsymbol{I}_s = \int_{-\infty}^{+\infty} \boldsymbol{f}(x)\,dx \tag{A.9}$$

To account accurately for the contribution of the pole at $x = x_0$ extract the singular part of integrand in the explicit form

$$\boldsymbol{I}_s = \operatorname{res}\{f(x_0)\}\int_{-\infty}^{+\infty}\frac{dx}{x-x_0} + \int_{-\infty}^{+\infty}\left(\boldsymbol{f}(x) - \frac{\operatorname{res}\{f(x_0)\}}{x-x_0}\right)dx. \quad \text{(A.10)}$$

The exact value of the first integral in (A.10) equals $\pi i * \operatorname{sign}(\operatorname{Im} x_0)$ where $\operatorname{sign}(\operatorname{Im} x_0) = \pm 1$ as $\operatorname{Im} x_0 \to \pm 0$. The integrand of the second integral is a regular function. Thus a one-point rectangular rule quadrature lends itself here to merge the integration into a summation

$$\boldsymbol{I}_s \simeq \pi i * \operatorname{sign}(\operatorname{Im} x_0) * \operatorname{res}\{\boldsymbol{f}(x_0)\} + \sum_{n=-\infty}^{+\infty}\left(\boldsymbol{f}(y_n) - \frac{\operatorname{res}\{f(x_0)\}}{y_n - x_0}\right), \quad \text{(A.11)}$$

where $y_n = (n-1/2)\pi/\boldsymbol{L}$ and $\boldsymbol{L}$ is a sampling scale. Hence choosing $\boldsymbol{L}$ in such a way that none of y_n coincides with x_0 and making use of the equality

$$\sum_{n=-\infty}^{+\infty}\frac{1}{y_n - x_0} = \pi tg(\pi x_0)$$

we obtain the numerical quadrature for infinite singular integral

$$I_s \simeq \pi i * \operatorname{res}\{f(x_0)\} * (\operatorname{sign}(\operatorname{Im} x_0) + itg(\pi x_0)) + \sum_{n=-\infty}^{+\infty} f(y_n). \quad \text{(A.12)}$$

It is necessary to emphasize that the series of (A.12) would be just the same as if we treated a problem associated with a shielded structure. Therefore the magnitude of $\boldsymbol{L}$ used to be taken greater than a generic scale of discontinue area S.

C. The main principles of the above approach underlie the treatment of the sets of the two-dimensional integral equation (2) and (19), (20). We present below some sets of the expansion bases for areas S of both a specific and an arbitrary shapes. The weight factors account explicitly for the edge condition wherever except for the corners.

1) S is a rectangular with vertexes at $x_c = \pm 1_x$, $z_c = \pm 1_z$: The complete orthonormalized set in a space domain takes the form

$$\tilde{\eta}_x^{jq}(x,z) = C_j^{\tau}(x/1_x) * \left(1_x^2 - x^2\right)^{\tau-1/2} * C_q^{\tau+1}(z/1_z) * \left(1_z^2 - z^2\right)^{\tau+1/2} \qquad q,j = 0,1\cdots$$
$$\tilde{\eta}_z^{jq}(x,z) = C_j^{\tau+1}(x/1_x) * \left(1_x^2 - x^2\right)^{\tau+1/2} * C_q^{\tau}(z/1_z) * \left(1_z^2 - z^2\right)^{\tau-1/2} \quad \text{(A.13)}$$

where $\boldsymbol{C}_j^{\tau}(x)$ is Gegenbauer's polynomial; index τ is associated with the edge condition at the verge of S. In the case of perfect conductors $\tau = 0$, and $\boldsymbol{C}_j^{o}(x)$, $\boldsymbol{C}_j^{1}(x)$ can be rearranged to Chebyshev's polynomials of the first $\boldsymbol{T}_j(x)$ and second $\boldsymbol{U}_j(x)$ kind, respectively.

The Fourier transformation of (A.13) yields the corresponding formulations in spectral domain

$$\boldsymbol{u}_{jq}^{e}(\alpha,\beta) = \boldsymbol{J}_{j+\tau-1/2}(\alpha l_x) * \alpha^{-(\tau-1/2)} * \boldsymbol{J}_{q+\tau+1/2}(\beta l_z) * \beta^{-(\tau+1/2)}, \qquad q,j = 0,1\cdots$$
$$\boldsymbol{u}_{jq}^{m}(\alpha,\beta) = J_{j+\tau+1/2}(\alpha l_x) * \alpha^{-(\tau+1/2)} * \boldsymbol{J}_{q+\tau-1/2}(\beta l_z) * \beta^{-(\tau-1/2)} \quad \text{(A.14)}$$

2) S is a parallelogram with the vertexes at $x_c = \pm 1_x$, $z_c = \pm 1_z + x_c \operatorname{ctg}\varphi$, where φ is an acute angle at a vertex [8].

The complete orthonormalized set in space domain is as follows

$$\tilde{\eta}_x^{jq}(x,z) = \boldsymbol{T}_j(x/l_x)/\sqrt{l_x^2 - x^2} * \boldsymbol{U}_q(z/l_z) * \sqrt{l_z^2 - (t(x,z))^2},$$
$$\tilde{\eta}_z^{jq}(x,z) = \boldsymbol{U}_j(x/l_x) * \sqrt{l_x^2 - x^2} * \boldsymbol{T}_q(z/l_z) \div \sqrt{l_z^2 - (t(x,z))^2}, \quad \text{(A.15)}$$

where $t(x,z) = z - x * \operatorname{ctg}\varphi$. The corresponding formulations of basis functions in spectral domain are as follows

$$\boldsymbol{u}_{jq}^{e}(\alpha,\beta) = \boldsymbol{J}_{q+1}(\beta l_z)/\beta * \boldsymbol{J}_j\left(\alpha^{+} l_x\right),$$
$$\boldsymbol{u}_{jq}^{m}(\alpha,\beta) = \boldsymbol{J}_q(\beta l_z) * \boldsymbol{J}_{j+1}\left(\alpha^{+} l_x\right)/\alpha^{+}, \quad \text{(A.16)}$$

where $\alpha^{+} = \alpha + \beta * \operatorname{ctg}\varphi$.

3) Disk-shaped area S with a radius R: Analytical form of the complete orthonormalized set of basis functions is known only for spectral domain [9]

$$\boldsymbol{u}_{jq}^{e,m}(\alpha,\beta) = \Phi_{jq}^{e,m}(\rho)\exp(ij\theta), \qquad q,j = 0,1,\cdots \quad \text{(A.17)}$$

where

$$\Phi_{jq}^{e}(\rho) = \boldsymbol{J}_{2q+j+\tau-1/2}(\rho R) * \rho^{-(\tau-1/2)}$$
$$\Phi_{jq}^{m}(\rho) = \boldsymbol{J}_{2q+j+\tau+1/2}(\rho R) * \rho^{-(\tau+1/2)} \quad \text{(A.18)}$$

$\alpha = \rho\cos\theta$, $\beta = \rho\sin\theta$; index τ is determined by the edge condition nearby a verge of S. $\tau = 0$ corresponds to the perfect conductors. It is important to note that the basis functions for axisymmetric problems are orthogonal with respect to index j.

4) Ellipse with semi-axes l_x and l_z [17]. Basis functions for ellipse takes the form (A.17), (A.18) in which ρR is replaced by $\rho_\iota = \sqrt{(\alpha l_x)^2 + (\alpha l_z)^2}$.

5) Ring-shaped area S: $R - l \le r \le R + l$ [18], [21]: Basis functions defined in spectral domain take the form (A.17) with

$$\Phi_{jq}^{e}(\rho) = \boldsymbol{J}_q^j(-1/2,\rho) \qquad \Phi_{jq}^{m}(\rho) = \frac{d}{\rho\, d\rho}\boldsymbol{J}_q^j(-1/2,\rho) \quad \text{(A.19)}$$

where $\boldsymbol{J}_q^j(\tau,\rho) = \rho^{-(\tau+1/2)}\boldsymbol{J}_{n(q)+\tau+1/2}(\rho 1) * \boldsymbol{J}_{m(q)+j}(\rho R)$, $n(q) = [3q - 2 - (-1)^q(q-2)]/4$, $m(q) = q[1 + (-1)^q]/4$; $\alpha = \rho\cos\theta$, $\beta = \rho\sin\theta$.

6) Perfect conducting patch S of arbitrary shape [24]. Basis functions are defined in space domain as follows

$$\tilde{\eta}_x^{jq}(x,z) = \boldsymbol{T}_j(x/l_q)/\sqrt{l_q^2 - x^2} * \sigma_q(z) \qquad q,j = 0,1,\cdots$$
$$\tilde{\eta}_z^{jq}(x,z) = \boldsymbol{U}_j(x/l_q) * \sqrt{l_q^2 - x^2} * \sigma_q(z) \quad \text{(A.20)}$$

where $\sigma_q(z)$ are splines with abscissas in the points z_q, $l_q = w_q/2$ $(w_q = w(z_q))$ is a width of patch or aperture in the section $z = z_q$.

ACKNOWLEDGMENT

Authors are grateful to the referees for helpful suggestions and their constructive criticism.

REFERENCES

[1] W. J. R. Hoefer, "New horizons in numerical time domain modeling of microwave structures," in *Proc. 20th European Microwave Conf.,* 1990, Budapest, pp. 7–20.

[2] I. Wolff, "From approximations to a three-dimensional full-wave solution of planar line discontinuities for microwave integrated circuits," in *Proc. MicroColl Workshop,* 1990, Budapest, pp. 123–140.

[3] T. Itoh, *Numerical Technique for Microwave and Millimeter-wave Passive Structures.* New York, Wiley, 1989.

[4] R. N. Jansen "The spectral domain approach for microwave integrated circuits," *IEEE Trans. Microwave Theory Tech.,* vol. MTT-33, pp. 1043–1056, Oct. 1985.

[5] G. F. Zargano *et al., Transmission Lines of Complex Cross-Section,* in Russian. Rostov-on-Don, USSR: Rostov State University Press, 1983.

[6] R. Jansen, "High-order finite element polynomials in the computer analysis of arbitrary shaped microstrip resonators," Arch. Elek. Übertrangung, vol. 30, pp. 71–79, 1976.

[7] S. Marchetti and T. Rozzi, "Electric field singularities in microwave integrated circuits (MIC)," in *Proc. 20th European Microwave Conf.,* 1990, Budapest, pp. 823–828.

[8] A. M. Lerer, "Discontinuities in finlines," *Radio Eng. Electron. USSR,* vol. 31, pp. 2129–2136, Nov. 1986.

[9] R. F. Fikhmanas and P. Sh. Fridberg, "Analytical properties of Hankel transformation and their application for numerical realization of variational principals," *Radio Eng. Electron. USSR,* vol. 23, pp. 1625–1630, Aug. 1978.

[10] A. B. Rozenblyum and P. Sh. Fridberg, "Calculation of linear functionals for the class of axisymmetric problems of field theory," *Radio Eng. Electron. USSR,* vol. 31, pp. 1057–1065, June 1986.

[11] K. Wu and R. Vahldieck, "A new method of modeling three-dimensional MIC/MMIC circuits: The space–spectral domain approach," *IEEE Trans. Microwave Theory Tech.,* vol. MTT-38, pp. 1309–1318, Sept. 1990.

[12] T. Becks and I. Wolff, "Improvements of spectral domain analysis technique for arbitrary planar circuits," in *Proc. 20th European Microwave Conf.,* 1990, Budapest, pp. 1015–1020.

[13] E. El-Sharawy and R. W. Jackson, "Full wave analysis of an infinitely long magnetic surface wave transducer," *IEEE Trans. Microwave Theory Tech.,* vol. MTT-38, pp. 730–738, June 1990.

[14] A. M. Lerer, V. S. Mikchalevskyi, and A. G. Schuchinsky, "Electrodynamic theory of microstrip line on ferrite substrate," *Radio Eng. Electron. USSR,* vol. 29, pp. 1039–1048, June 1984.

[15] A. M. Lerer, "Solution of dual integral equations in the problems of microstrip and slot lines," *Radiophys. Quant. Electron., Trans. Higher School USSR,* vol. 28, pp. 507–512, Apr. 1985.

[16] A. S. Omar and K. F. Schunemann, "Analysis of waveguides with metal inserts," *IEEE Trans. Microwave Theory Tech.,* vol. MTT-37, pp. 1924–1932, Dec. 1989.

[17] A. M. Lerer, "Accounting edge condition at the verge of elliptic shape disk for solving some boundary value problems of microwave field theory," *Radio Eng. Electron. USSR,* vol. 32, pp. 1418–1425, July 1987.

[18] P. Sh. Fridberg, A. M. Lerer and G. N. Shelamov, "Investigation on ring planar structures," in *Proc. URSI Int. Symp on Electromagnetic Theory,* 1989, Stockholm, pp. 539–541.

[19] B. A. Gribnikov, V. N. Ivanov, A. M. Lerer, A. G. Schuchinsky, and G. N. Shelamov, "Microwave ferrite structures—Finlines and resonators," in *Proc, 18th European Microwave Conf.,* 1988, Stockholm, pp. 1105–1111.

[20] B. A. Gribnikov, V. A. Kuznetsov, and A. G. Schuchinsky, "Tunable microwave ferrite resonators," in *Proc. 20th European Microwave Conf.,* 1990, Budapest, pp. 1145–1150.

[21] V. I. Kravchenko, A. M. Lerer, and G. N. Shelamov, "Theoretical and experimental investigation of opened and shielded ring (disk) shaped planar structures," *Radio Eng. Electron. USSR,* vol. 35, pp. 673–686, Apr. 1990.

[22] A. M. Lerer, V. M. Lerer, V. D. Ryazanov, and V. A. Sledkov, "Theory and application of planar transmission lines with periodic structures at the edges," in *Proc. URSI Int. Symp. on Electromagnetic Theory,* 1989, Stockholm, pp. 550–552.

[23] A. M. Lerer, V. S. Mikchalevskyi, and I. N. Semenikhin, "Diffraction of waveguide waves on the opening in common wall of rectangular waveguides," in *Proc. SMBO-91 Int. Microwave Conf.: Microwaves: Trends to Future,* Rio de Janeiro, 1991.

[24] R. Sorrentino, T. Itoh, "Transverse resonance analysis of finline discontinuities," *IEEE Trans. Microwave Theory Tech.,* vol. MTT-33, pp. 1633–1638, Dec. 1984.

[25] J. Schwinger, and D. S. Saxon, *Discontinuities in Waveguides.* NY: Gordon and Breach, 1968.

[26] K.-S. Kong and T. Itoh, "Computer-aided design of evanescent mode waveguide bandpass filter with nontouching E-Plane fins," *IEEE Trans. Microwave Theory Tech.,* vol. MTT-37, pp. 1998–2004, Dec. 1989.

[27] H. A. Bethe, "Theory diffraction by small holes," *Phys. Rev.,* vol. 66, pp. 163–182, 1944.

[28] Kh. L. Garb, R. S. Meyerova, G. V. Pochikaev, and P. Sh. Fridberg, "Diffraction H_{10}-wave by rectangular aperture in common wide wall between couple of rectangular waveguides," *Radio Eng. Electron. USSR,* vol. 34, pp. 1150–1157, June 1989.

[29] S. R. Rengarajan, "Analysis of centered-inclined waveguide slot coupler," *IEEE Trans. Microwave Theory Tech.,* vol. MTT-37, pp. 884–889, May 1989.

[30] S. R. Rengarajan, "Characteristics of a longitudinal/transverse coupling slot in crossed rectangular waveguides," *IEEE Trans. Microwave Theory Tech.,* vol. MTT-37, pp. 1171–1177, Aug. 1989.

[31] L. A. Weinstein, *The Theory of Diffraction and the Factorization Method.* Boulder: Golem Press, 1969.

[32] B. A. Gribnikov, V. N. Ivanov, V. A. Kuznetsov, A. M. Lerer, and A. G. Schuchinsky, "Thin film dielectric waveguide on layered gyrotropic substrate," *Radio Eng. Electron. USSR,* vol. 33, pp. 29–36, Jan. 1988.

[33] V. A. Kuznetsov and A. M. Lerer, "Resonant frequencies of disk-shaped dielectric resonators," *Radio Eng. Electron. USSR,* vol. 29, pp. 2124–2128, Nov. 1984.

[34] I. I. Vorovich, V. M. Alexandrov, and V. A. Babeshko, *Nonclassical Mixed Boundary Problems in the Theory of Elasticity,* in Russian. Moscow: Nauka, 1974.

[35] G. F. Zargano, A. M. Lerer, V. S. Mikhalevsky, and G. P. Sinyavsky, "Application of mode matching technique accounting for the edge condition to the problems of waveguides of Π- and cross-shape cross sections," *Radio Eng. Electron. USSR,* vol. 22, pp. 2068–2073, Oct. 1977.

[36] V. P. Lyapin, V. S. Mikhalevsky, and G. P. Sinyavsky, "Taking into account the edge condition in the problem of diffraction waves on step discontinuity in plane waveguide," *IEEE Trans. Microwave Theory Tech.,* vol. MTT-30, pp. 1107–1109, July 1982.

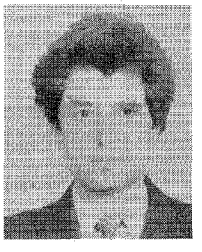

Alexander M. Lerer was born in Rostov-on-Don, USSR, on May 1, 1946. He received the M.Sc. and Ph.D. degrees in radiophysics from Rostov State University (USSR) in 1968 and 1974, respectively, and the D.Sc. degree from Saratov State Universities (USSR) in 1989.

In 1976 he was awarded the academic title of Senior Research Scientist. Since 1969 he has worked for Microwave Electrodynamics Laboratory at Rostov State University. In 1991 he was elected Professor of The Department of Applied Electrodynamics and Computer Modeling of Rostov State University. His research interests include development of numerical-analytical methods for the problems of microwave field theory; numerical modeling and investigations of planar, dielectric and waveguide transmission lines, resonators, and discontinuities of microwave and millimeter-wave circuits.

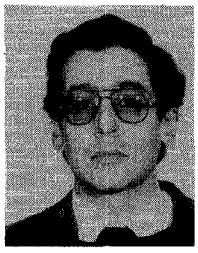

Alexander G. Schuchinsky was born in Rostov-on-Don, USSR, on October 19, 1951. He received the M.Sc. and Ph.D. degrees in radiophysics from Rostov State University in 1973 and Leningrad Electrical Engineering Institute (USSR) in 1983, respectively.

In 1988 he was awarded the academic title of Senior Research Scientist. Since 1973 he has worked for Microwave Electrodynamics Laboratory at Rostov State University. His research interests include development of numerical-analytical methods for the problems of microwave field theory, investigations of planar and waveguide structures with ferrite loading, and electrodynamic aspects of the theory of magnetostatic and spin waves in thin ferrite layers.